X-ray micro-tomography for investigations of brain tissues on cellular level

Anna Khimchenko[a*], Georg Schulz[a], Hans Deyhle[a], Peter Thalmann[a], Irene Zanette[b], Marie-Christine Zdora[b,c], Christos Bikis[a], Alexander Hipp[d], Simone E. Hieber[a], Gabriel Schweighauser[e], Jürgen Hench[e], and Bert Müller[a]

[a] Biomaterials Science Center, Department of Biomedical Engineering, University of Basel, Gewerbestrasse 14, 4123 Allschwil, Switzerland;
[b] Diamond Light Source Ltd, Diamond House, OX11 0DE Didcot, Oxfordshire, UK;
[c] Department of Physics and Astronomy, University College London, Gower Street, WC1E 6BT London, UK;
[d] Helmholtz-Zentrum Geesthacht, Max-Planck-Strasse 1, 21502 Geesthacht, Germany;
[e] Institute of Pathology, Department of Neuropathology, Basel University Hospital, Schönbeinstrasse 40, 4056 Basel, Switzerland

ABSTRACT

X-ray imaging in absorption contrast mode is well established for hard tissue visualization. However, performance for lower density materials is limited due to a reduced contrast. Our aim is three-dimensional (3D) characterization of micro-morphology of human brain tissues down to (sub-)cellular resolution within a laboratory environment. Using the laboratory-based microtomography (µCT) system nanotom® m (GE Sensing & Inspection Technologies GmbH, Wunstorf, Germany) and synchrotron radiation at the Diamond-Manchester Imaging Branchline I13-2 (Diamond Light Source, Didcot, UK), we have acquired 3D data with a resolution down to 0.45 µm for visualization of a human cerebellum specimen down to cellular level. We have shown that all selected modalities, namely laboratory-based absorption contrast micro-tomography (LBµCT), synchrotron radiation based in-line single distance phase contrast tomography (SDPR) and synchrotron radiation based single-grating interferometry (GI), can reach cellular resolution for tissue samples with a size in the mm-range. The results are discussed qualitatively in comparison to optical microscopy of haematoxylin and eosin (H&E) stained sections. As phase contrast yields to a better data quality for soft tissues and in order to overcome restrictions of limited beamline access for phase contrast measurements, we have equipped the µCT system nanotom® m with a double-grating phase contrast set-up. Preliminary experimental results of a knee sample consisting of a bony part and a cartilage demonstrate that phase contrast data exhibits better quality compared to absorption contrast. Currently, the set-up is under adjustment. It is expected that cellular resolution would also be achieved. The questions arise (1) what would be the quality gain of laboratory-based phase contrast in comparison to laboratory-based absorption contrast tomography and (2) could laboratory-based phase contrast data provide comparable results to synchrotron radiation based phase contrast data.

Keywords: X-ray micro-tomography, phase contrast, absorption contrast, grating interferometry, synchrotron radiation, brain tissue, cerebellum.

1. INTRODUCTION

Human brain belongs to the most impressive[1] organs within the body and its disorders are a severe health problem of a modern ageing society.[2] Being diverse in macroscopic symptoms, neurodegenerative disorders have much in common on (sub-)cellular level: loss of cells, demyelination or damage of cell axons.[3] There are many open questions in the field. For example, exact causes and key clinical features of a degenerative process, such as the role of metal ions,[4–6] are not clear; knowledge about neuroanatomical connections is limited as well.[7] Thus, high-resolution three-dimensional (3D) visualization of brain tissue can be highly beneficial.[8]

* anna.khimchenko@unibas.ch; phone: +41 61 207 54 41; fax: +41 61 207 54 99; bmc.unibas.ch

Developments in X-Ray Tomography X, edited by Stuart R. Stock, Bert Müller, Ge Wang, Proc. of SPIE Vol. 9967, 996703 · © 2016 SPIE · CCC code: 0277-786X/16/$18 · doi: 10.1117/12.2237554

The structure of brain and nervous system is complex,[9,10] having a 3D multi-scale hierarchical organization. Thus, characterization of volumes is desirable over thin sections. Nevertheless, within a laboratory environment remains a gap in large-scale 3D imaging techniques that provides high spatial resolution and density contrast for soft tissues. Serial sectioning or block-face methods[11,12] require a complex volume reconstruction,[13] do not provide isotropic resolution, are destructive, time-consuming, and often related to a significant tissue loss, stress, and strain. Sectioning-free methods combined with tissue-transformation[14,15] are expensive, time-consuming and cause local changes within inhomogeneous tissues.

The conventional approach for visualization of soft tissues with a cellular resolution within a laboratory environment remains optical microscopy,[16,17] see Figure 1. Apart from possible slicing or staining artifacts (Fig. 1 steps 5 - 8), this methodology is highly time-consuming, making it almost impossible to cover the complete 3D micro-architecture.[18–20] In addition, this methodology is destructive (Fig. 1 step 5).[17]

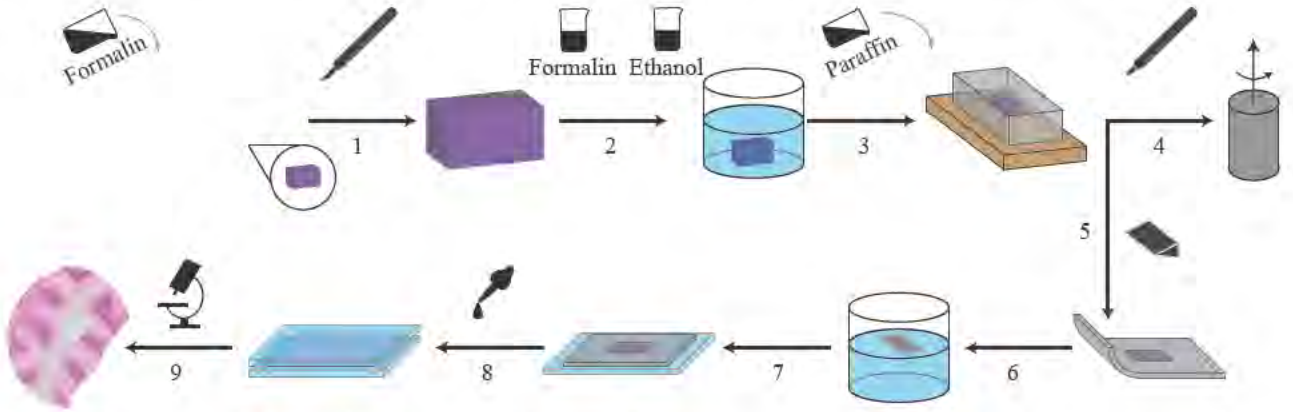

Figure 1. Imaging work flow: schematic representation of the specimen preparation for optical microscopy examination (steps 1 - 3 and 5 - 9) and tomography (steps 1 - 4). 1: specimen dissection; 2: fixation and dehydration; 3: paraffin embedding; 4: punching of a cylinder; 5: sectioning by microtome; 6, 7: mounting of a thin section on a glass slide; 8: staining; 9: optical microscopy examination.

At the same time, X-ray imaging modalities can offer cellular resolution for large tissue volumes in a non-destructive manner.[21–25] In this communication, we discuss methods for soft tissue visualization suitable for extracting cellular information within a laboratory environment. Comparing laboratory-based absorption contrast data of formalin-fixed paraffin-embedded (FFPE) human cerebellum specimen to selected synchrotron radiation based phase contrast modalities, one can see that data quality is comparable. It is expected that extending laboratory-based μCT system towards phase contrast will yield further data quality increase. The open questions remain (1) what is the quality gain in comparison to laboratory-based absorption contrast tomography and (2) could laboratory-based phase contrast data provide a comparable result to the synchrotron radiation based phase contrast data.

2. MATERIALS AND METHODS

2.1 Specimen preparation

The human cerebellum block from a 73-year-old male body was visualized *post mortem*. Informed consent for scientific use was obtained and all procedures were conducted in accordance with the Declaration of Helsinki and approved by the Ethikkommission Nordwestschweiz. The specimen preparation and paraffin embedding were performed based on the standard histological protocols (Fig. 1 steps 1 - 3), for more details see.[21,26] After paraffin embedding the tomography specimen with 4.0 mm height and 2.6 mm diameter was extracted with a metal punch (Fig. 1 step 4).

The femoratibial articular surface of the lateral femur condyle of the left knee joint was extracted from a donated body of a 87 years-old female, for more details see.[27] All steps were conducted in accordance with the Declaration of Helsinki and according to the ethical guidelines of the Canton Basel.

2.2 Laboratory-based absorption contrast micro-tomography

Laboratory-based absorption contrast micro-tomography ($LB_{\mu}CT$) was carried out on nanotom® m (GE Sensing & Inspection Technologies GmbH, Wunstorf, Germany) equipped with a 180 kV / 15 W nanofocus® tube with tungsten target.[28,29] The experimental parameters are summarized in Table 1. To increase the flux, the detector was moved close to source position, corresponding to the focus-detector distance FDD 255 mm, and sample close to source position, corresponding to the focus-object distance FOD 4.94 mm. Data acquisition and reconstruction were performed with datos|x 2.0 software (phoenix|x-ray, GE Sensing & Inspection Technologies GmbH, Wunstorf, Germany). The reconstructed slices were median filtered using VGStudio MAX 2.1 (Volume Graphics, Heidelberg, Germany) for a noise reduction (median filter size 3 × 3).

Table 1. Parameters of tomography methods. $LB_{\mu}CT$: laboratory-based absorption contrast micro-tomography; LBGI: laboratory-based grating interferometry; GI_8: synchrotron radiation based single grating with a period 8 µm phase contrast interferometry; GI_{10}: synchrotron radiation based single grating with a period 10 µm phase contrast interferometry; $SDPR_{1.1}$: synchrotron radiation based in-line single distance phase contrast tomography with an effective pixel size 1.1 µm; $SDPR_{0.45}$: synchrotron radiation based in-line single distance phase contrast tomography with an effective pixel size 0.45 µm; l: effective pixel size; W: beam parameters; U: tube acceleration voltage; I: tube current; E: photon energy; №: number of projections; t_{exp}: exposure time; $t_{exp}{}^{*}$: exposure time for a single phase step; d_p: sample detector distance; d_i: inter-grating distance; α: scanning angle range.

	l [µm]	W	№	t_{exp} [s]	d_p [cm]	d_i [cm]	α [deg.]
$LB_{\mu}CT$	2.20	$U = 60$ kV, $I = 310$ kV	1440	2.00	22.00		360.0
LBGI	23.22	$U = 42$ kV, $I = 310$ kV	400	9.00*		29.60	240.6
GI_8	1.10	$E = 19$ keV	1200	3.00*		58.30	180.0
GI_{10}	2.30	$E = 19$ keV	1200	3.00*		72.00	180.0
$SDPR_{1.1}$	1.10	$E = 19$ keV	2400	1.58	8.50		360.0
$SDPR_{0.45}$	0.45	$E = 19$ keV	2400	8.00	5.00		360.0

2.3 X-Ray micro-tomography in phase contrast mode

Figure 2 shows experimental arrangements for phase contrast tomography. The special optical elements, such as gratings, are required only for the grating-based methods (Fig.2 A - F).

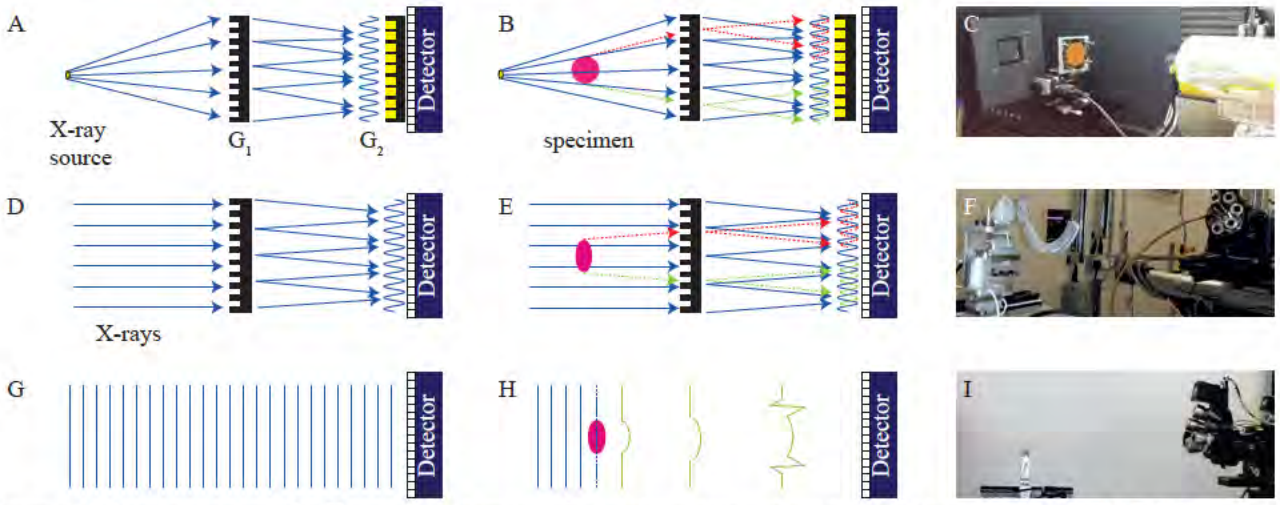

Figure 2. Schematic set-ups for X-ray micro-tomography in phase contrast mode with photographs. A, B, C: laboratory-based double-grating interferometry; D, E, F: synchrotron radiation based single-grating interferometry; G, H, I: synchrotron radiation based in-line single distance tomography. G_1: phase grating; G_2: analyser grating.

2.3.1 Laboratory-based double-grating interferometry

In order to extend capabilities of the nanotom® m toward phase contrast, it was equipped with a double-grating interferometric set-up, for more details see.[30] Laboratory-based double-grating (LBGI) measurement was performed with parameters summarized in Table 1. The source operation mode was set to *"mode 1"*, corresponding to an estimated source size of 2 µm, as specified by the supplier. Due to a sufficiently small source size the source grating (G_0) was not required. Measurements in single-grating configuration were not possible and the analyser grating (G_2) was required for the set-up as the detector is not able to resolve the interference pattern.

Figure 2 A - C shows experimental set-up for a cone-beam laboratory-based double-grating interferometry. The distance between the gratings corresponds to the 1st Talbot order. The gratings were fabricated for a design energy of 30 keV (microworks GmbH, Karlsruhe, Germany). A phase-stepping technique was used.[31] Grating G_1 was scanned over 2 periods of interference pattern in 11 phase steps. The phase recovery and tomographic reconstruction of the data were carried out in Matlab R2014a (MathWorks, Natick, USA).

2.3.2 Synchrotron radiation based single-grating interferometry

Figure 2 D - E schematically shows the set-up for synchrotron radiation based single-grating interferometry (GI) and Figure 2 F photograph of the set-up. GI of a human cerebellum specimen was performed at Diamond-Manchester Imaging Branchline I13-2 (Diamond Light Source, Didcot, UK).[32] A monochromatic X-ray beam was extracted from a silicon <111> double crystal monochromator. After being transmitted through the sample, the X-ray beam was collected by a scintillator-based X-ray detector pco.4000 (PCO AG, Kelheim, Germany) with 4× and 2× optical magnifications, with 2 single-grating set-ups: GI_8 and GI_{10}, for more details see Table 1. For both set-ups the distance between the gratings corresponds to the 1st Talbot order. The absence of a water tank in the set-up caused phase wrapping between the sample and air. Thus a "no-tank correction" was performed before phase retrieval.[33] Data processing and reconstruction were performed in a similar to LBGI manner.

2.3.3 Synchrotron radiation based in-line single distance tomography

Synchrotron radiation based in-line single distance phase contrast imaging of a human cerebellum specimen was performed at Diamond-Manchester Imaging Branchline I13-2 using a pco.4000 detector. The effective pixel sizes were 0.45 µm ($SDPR_{0.45}$) and 1.1 µm ($SDPR_{1.1}$) depending on the optical magnification of the scintillator-based detector. Since the specimen diameter was bigger for the effective pixel size of 0.45 µm than effective field of view (FOV), measurement was performed in a local tomography configuration. Flat-field and dark-current corrections, zero-padding, and phase recovery of tomography data were performed using the software tool ANKAphase[34] with an input parameter $\delta/\beta = 2406$[21] for 1.1 µm effective pixel size and $\delta/\beta = 414$ for 0.45 µm effective pixel size. The second δ/β value was decreased in order to reduce gradient artefacts in the data based on qualitative assessment. The tomographic reconstruction was done in Matlab R2014b (Simulink, The MathWorks, Inc., USA).

2.3.4 Data registration

For the comparison of tomography data acquired with selected modalities, datasets were registered using automatic 3D/3D registration tool[19,35] with rigid transformation constraints. The SDPR with effective pixel size 1.1 µm was set as reference dataset.

3. RESULTS AND DISCUSSION

3.1 Phase contrast versus absorption contrast

Figure 3 presents selected registered tomographic slices measured by LBµCT (A, D), GI_{10} (B, E) and $SDPR_{1.1}$ (C, F) with line profiles. The figure shows for each imaging modality one selected slice of a human cerebellum specimen with a magnification. Magnifications in Figure 3 E - F are cropped around the region occupied by structures of interest. Visual inspection of the registered slices reveals that *Stratum granulosum*, *Stratum moleculare*, individual cells, and blood vessels within the white matter can be recognised for all modalities in a comparable manner. Intensity differentiation between *Stratum granulosum* and *Stratum moleculare*, which both belong to grey matter, can enable intensity-based segmentation of individual cerebellar layers. LBµCT data exhibits a higher level of noise, thus additional filtering is essential for a better feature extraction.

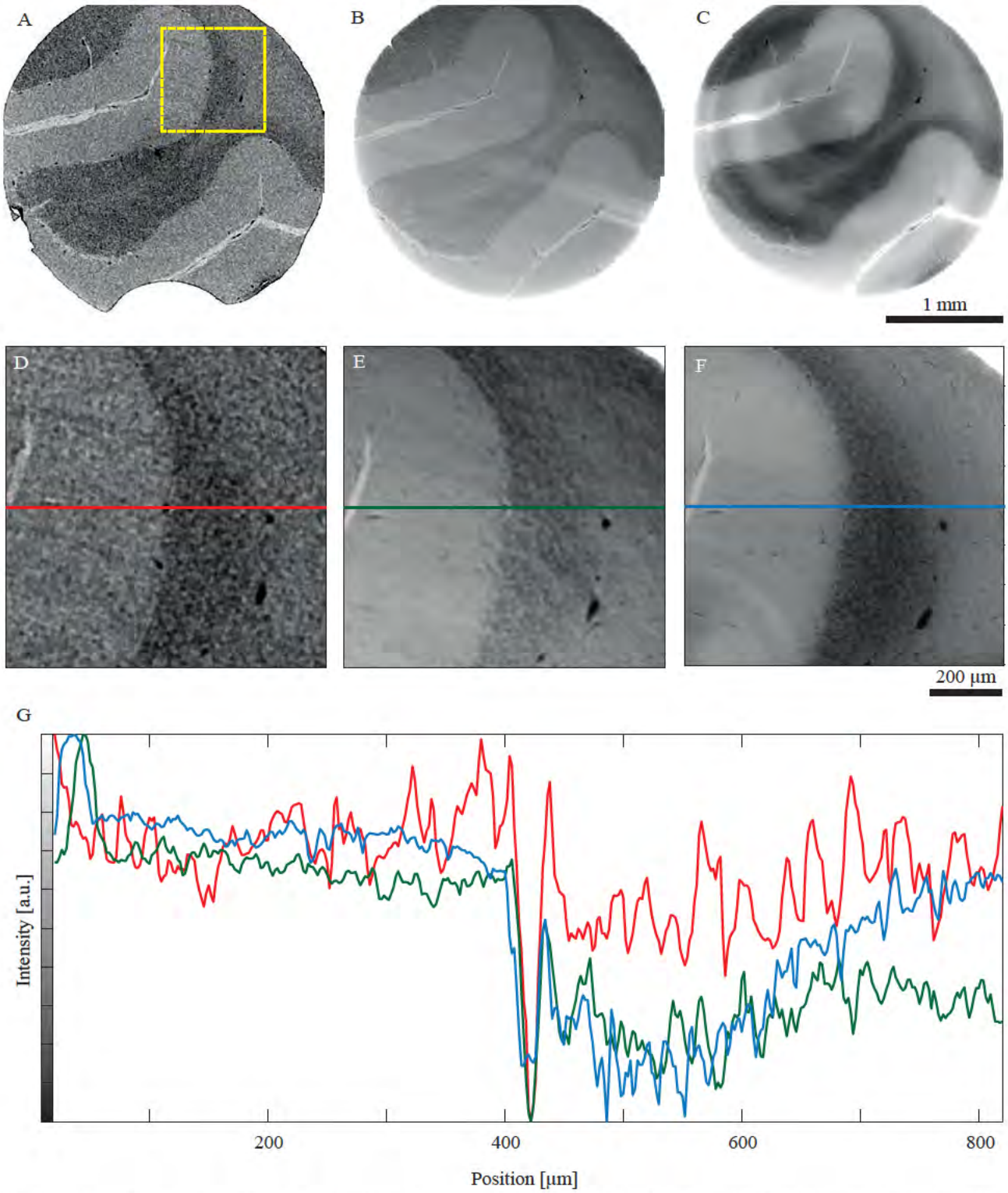

Figure 3. Selected registered tomographic slices measured by µCT in absorption contrast (A, D), synchrotron radiation based phase contrast interferometry with a grating period of 10 µm (B, E) and synchrotron radiation based in-line single distance phase contrast tomography with an effective pixel size of 1.1 µm. Line plot through the magnified part of slices (G) illustrates that modalities are comparable in terms of normalized intensity.

Currently available laboratory-based μCT systems can provide isotropic resolution[1] down to 300 nm. The limiting parameter for the successful visualization of soft tissue in the absorption mode is contrast.[1] Thus, for visualization of soft tissues, phase contrast is preferred due to a higher sensitivity.[17,36] It was recently demonstrated that FFPE brain tissues provide a contrast comparable to a conventional histology.[26] In this communication, we state that the data contrast is almost alike to a synchrotron radiation based phase contrast data.

3.2 Cellular visualization

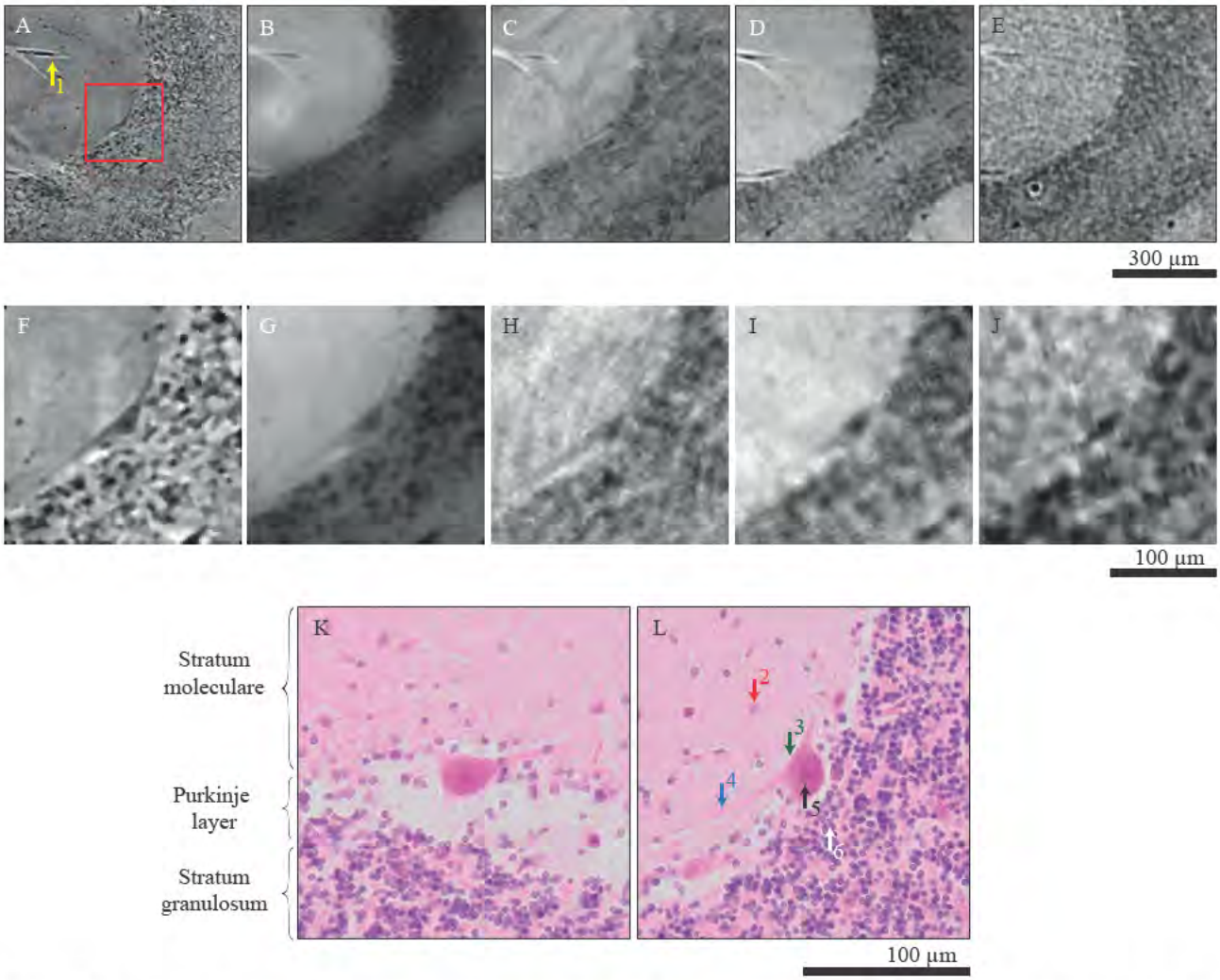

Figure 4. Hard X-ray images of a human cerebellum block showing a tomographic visualization of individual cells with magnification (A - J) and selected cropped histological sections (K - L). A, F: synchrotron radiation based in-line single distance phase contrast tomography with an effective pixel size of 0.45 μm; B, G: synchrotron radiation based in-line single distance phase contrast tomography with an effective pixel size of 1.1 μm; C, H: synchrotron radiation based phase contrast interferometry with a grating period of 8 μm; D, I: synchrotron radiation based phase contrast interferometry with a grating period of 10 μm; E, J: laboratory based absorption contrast μCT; K, L: histology. Yellow arrow (1): blood vessel; Red arrow (2): stellate cell; Green arrow (3): Purkinje cell with dendrite (4, blue); Black arrow (5): nucleus of Purkinje cell; White arrow (6): granular cell.

Figure 4 presents selected registered tomographic slices of a human cerebellum block showing individual cells with magnification (A - J). The tomographic slices are qualitatively compared to the equivalent images of a

FFPE human cerebellum obtained with optical microscopy of H&E-stained section.[26] Analysing Purkinje cells in cerebellum, we can see that in all modalities a comparable number of features can be discriminated, although, stellate cells are only visible in SDPR data. The highest level of detail was achieved for the Fig. 4 A/F and B/G, where one can distinguish cell bodies and neural fibers. This is related to the effective pixels size of the data.

Laboratory-based absorption contrast tomography of FFPE can reach cellular resolution.[26] With a pixel size of 2.2 µm it already enables visualization of the beginning of a dendrite tree, see Figure 4 J. The further increase of resolution can enable visualization of complete neuronal dendrite structures without dedicated contrast agent in 3D within a laboratory environment. It can be expected that laboratory-based absorption contrast tomography with decreased pixel size can enable quantification of the 3D neuronal dendrite structure, for example, bifurcation angles and density, dendritic tree size or fractal dimensions. The method can be used for the identification and quantification of a neural degeneration at early stages and that it has the potential of providing a powerful tool for the quantitative evaluation of cells changes in *post mortem* brain tissues.

3.3 Grating interferometry using laboratory system

Figure 5 shows first reconstruction results for laboratory-based double-grating phase contrast interferometry obtained for human knee sample, consisting of a bony part and a cartilage. The phase contrast slice is shown in Fig. 5 A, conventional absorption contrast in Fig. 5 B and dark-field in Fig. 5 C. Whereas the bony part of the sample looks very similar in the absorption (Fig. 5 B) and phase contrast (Fig. 5 A) images, a difference is visible in the cartilage, which is invisible in the absorption contrast.

Boundaries and interfaces produce a strong signal in the dark-field image.[37] As the bone part is highly porous, it is expected to be clearly visible in dark-field images. The marginal dark-field contrast can be explained by a low contrast-to-noise ratio (CNR) due to a limited number of projections and scanning angle range.

Grating-based phase contrast imaging can provide an important supplementary information to conventional absorption contrast, retrieving X-ray absorption, phase, and dark-field images simultaneously. Combining absorption, phase and dark-field, grating-based tomography offers a powerful multi-modal approach. In future, a further increase in the sensitivity could provide a required contrast for visualisation with a cellular resolution.

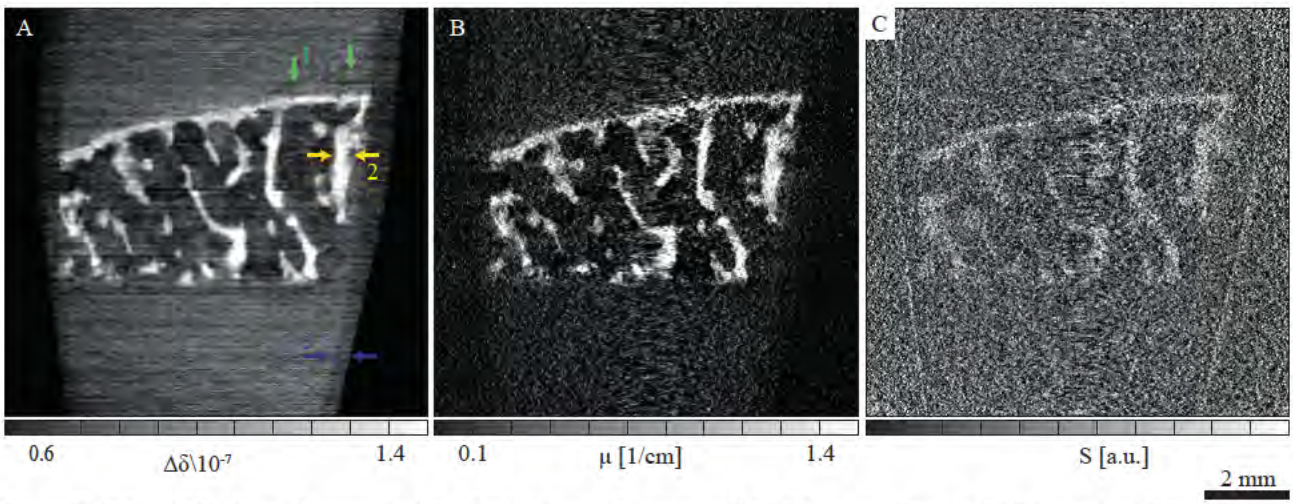

Figure 5. Selected horizontal cross-section of a knee sample measured by laboratory-based double-grating phase contrast tomography. A: phase contrast; B: absorption contrast; C: dark field. Green arrow (1): inhomogeneity in cartilage; Yellow arrow (2): bone structure; Blue arrow (3): container wall.

4. SUMMARY AND OUTLOOK

As it was recently shown, laboratory-based µCT of FFPE sample yields to the absorption contrast, comparable to a conventional histological sections.[26] In this work we have shown that laboratory-based µCT can also provide

data which is almost alike to synchrotron radiation based phase contrast, on the example of human cerebellum specimen.

It is highly beneficial to correlate morphological structures with their cellular functions.[38] X-rays are a powerful tool in non-destructive volumetric imaging of micromorphology. We suggest that laboratory-based tomography could be combined with optical microscopy to characterize 3D structure of soft materials.[39] Within this context, X-ray tomography enables the 3D visualisation and quantification of tissues prior to histological sectioning.[1,40]

In this work, we present selected tomography results of FFPE human cerebellum specimen at varying contrast and resolution. The highest resolution was achieved for synchrotron radiation based in-line single distance phased contrast tomography. We qualitatively compared selected tomography methods, reaching a cellular resolution. In order to identify the appropriate tomography approach to visualize micromorphology of soft tissue a more detailed comparison is required, which should include synchrotron radiation based double-grating interferometry with a water tank, synchrotron radiation based single-grating interferometry with a water tank, etc. Such a comparison should include instrumental and time requirements for data acquisition and reconstruction, as well as data quality and a potential for data combination.

5. ACKNOWLEDGEMENTS

The authors acknowledge the financial support of the Swiss National Science Foundation (SNSF) projects 147172 and SNSF R'Equip project 133802. The authors highly appreciated the assistance of the team of Diamond Synchrotron Radiation Facility, Didcot, UK, particularly Christoph Rau, Joan Vila-Comamala and Pierre Thibault.

REFERENCES

[1] Schulz, G., Weitkamp, T., Zanette, I., Pfeiffer, F., Beckmann, F., David, C., Rutishauser, S., Reznikova, E., and Müller, B., "High-resolution tomographic imaging of a human cerebellum: Comparison of absorption and grating-based phase contrast," *J. R. Soc. Interface* **7**(53), 1665–1676 (2010).

[2] Saba, L., [*Imaging in Neurodegenerative Disorders*], Oxford University Press, Great Clarendon street, Oxford, OX2 6DP (2015).

[3] Praet, J., Santermans, E., Reekmans, K., de Vocht, N., Le Blon, D., Hoornaert, C., Daans, J., Goossens, H., Berneman, Z., Hens, N., Van der Linden, A., and Ponsaerts, P., "Histological characterization and quantification of cellular events following neural and fibroblast(-like) stem cell grafting in healthy and demyelinated CNS tissue," *Methods Mol. Bio.* **1213**, 265–283 (2014).

[4] Miller, L., Wang, Q., Telivala, T., Smith, R., Lanzirotti, A., and Miklossy, J., "Synchrotron-based infrared and X-ray imaging shows focalized accumulation of Cu and Zn co-localized with -amyloid deposits in Alzheimer's disease," *J. Struct. Biol.* **155**(1), 30–37 (2006).

[5] Bourassa, M. and Miller, L., "Metal imaging in neurodegenerative diseases," *Metallomics* **4**(8), 721–738 (2012).

[6] Leskovjan, A., Lanzirotti, A., and Miller, L., "Amyloid plaques in PSAPP mice bind less metal than plaques in human Alzheimer's disease," *NeuroImage* **47**(4), 1215–1220 (2009).

[7] Papp, E., Leergaard, T., Csucs, G., and Bjaalie, J., "Brain-wide mapping of axonal connections: Workflow for automated detection and spatial analysis of labeling in microscopic sections," *Front. Neuroinform.* **10**, 11 (2016).

[8] Schulz, G., Weitkamp, T., Zanette, I., Pfeiffer, F., Müller-Gerbl, M., David, C., and Müller, B., "Asymmetric rotational axis reconstruction of grating-based X-ray phase contrast tomography of the human cerebellum," *Proc. SPIE* **8506**, 850604 (2012).

[9] Lichtman, J., Pfister, H., and Shavit, N., "The big data challenges of connectomics," *Nat. Neurosci.* **17**(11), 1448–1454 (2014).

[10] Kasthuri, N., Hayworth, K., Berger, D., Schalek, R., Conchello, J., Knowles-Barley, S., Lee, D., Vázquez-Reina, A., Kaynig, V., Jones, T., Roberts, M., Morgan, J., Tapia, J., Seung, H., Roncal, W., Vogelstein, J., Burns, R., Sussman, D., Priebe, C., Pfister, H., and Lichtman, J., "Saturated reconstruction of a volume of neocortex," *Cell* **162**(3), 648–661 (2015).

[11] Oh, S. W., Harris, J. A., Ng, L., Winslow, B., Cain, N., Mihalas, S., Wang, Q., Lau, C., Kuan, L., Henry, A. M., Mortrud, M. T., Ouellette, B., Nguyen, T. N., Sorensen, S. A., Slaughterbeck, C. R., Wakeman, W., Li, Y., Feng, D., Ho, A., Nicholas, E., Hirokawa, K. E., Bohn, P., Joines, K. M., Peng, H., Hawrylycz, M. J., Phillips, J. W., Hohmann, J. G., Wohnoutka, P., Gerfen, C. R., Koch, C., Bernard, A., Dang, C., Jones, A. R., and Zeng, H., "A mesoscale connectome of the mouse brain," *Nature* **508**(7495), 207–214 (2014).

[12] Ichimura, K., Miyazaki, N., Sadayama, S., Murata, K., Koike, M., Nakamura, K.-I., Ohta, K., and Sakai, T., "Three-dimensional architecture of podocytes revealed by block-face scanning electron microscopy," *Sci. Rep.* **5**, 8993 (2015).

[13] Krauth, A., Blanc, R., Poveda, A., Jeanmonod, D., Morel, A., and Székely, G., "A mean three-dimensional atlas of the human thalamus: Generation from multiple histological data," *NeuroImage* **49**(3), 2053–2062 (2010).

[14] Chung, K., Wallace, J., Kim, S.-Y., Kalyanasundaram, S., Andalman, A. S., Davidson, T. J., Mirzabekov, J. J., Zalocusky, K. A., Mattis, J., Denisin, A. K., Pak, S., Bernstein, H., Ramakrishnan, C., Grosenick, L., Gradinaru, V., and Deisseroth, K., "Structural and molecular interrogation of intact biological systems," *Nature* **497**(7449), 332–337 (2013).

[15] Murray, E., Cho, J. H., Goodwin, D., Ku, T., Swaney, J., Kim, S.-Y., Choi, H., Park, Y.-G., Park, J.-Y., Hubbert, A., McCue, M., Vassallo, S., Bakh, N., Frosch, M. P., Wedeen, V. J., Seung, H. S., and Chung, K., "Simple, scalable proteomic imaging for high-dimensional profiling of intact systems," *Cell* **163**(6), 1500–1514 (2015).

[16] Krenkel, M., Markus, A., Bartels, M., Dullin, C., Alves, F., and Salditt, T., "Phase-contrast zoom tomography reveals precise locations of macrophages in mouse lungs," *Sci. Rep.* **5**, 9973 (2015).

[17] Lang, S., Zanette, I., Dominietto, M., Langer, M., Rack, A., Schulz, G., Le Duc, G., David, C., Mohr, J., Pfeiffer, F., Müller, B., and Weitkamp, T., "Experimental comparison of grating- and propagation-based hard X-ray phase tomography of soft tissue," *J. Appl. Phys.* **116**(15), 154903 (2014).

[18] Schulz, G., Morel, A., Imholz, M., Deyhle, H., Weitkamp, T., Zanette, I., Pfeiffer, F., David, C., Müller-Gerbl, M., and Müller, B., "Evaluating the microstructure of human brain tissues using synchrotron radiation-based micro computed tomography," *Proc. SPIE* **7804**, 78040F (2010).

[19] Müller, B., Deyhle, H., Lang, S., Schulz, G., Bormann, T., Fierz, F., and Hieber, S., "Three-dimensional registration of tomography data for quantification in biomaterials science," *Int. J. Mater. Res.* **103**(2), 242–249 (2012).

[20] Germann, M., Morel, A., Beckmann, F., Andronache, A., Jeanmonod, D., and Müller, B., "Strain fields in histological slices of brain tissue determined by synchrotron radiation-based micro computed tomography," *J. Neurosci. Meth.* **170**(1), 149–155 (2008).

[21] Hieber, S. E., Bikis, C., Khimchenko, A., Schweighauser, G., Hench, J., Chicherova, N., Schulz, G., and Müller, B., "Tomographic brain imaging with nucleolar detail and automatic cell counting," *Sci. Rep.* **6**, 32156 (2016).

[22] Zehbe, R., Haibel, A., Riesemeier, H., Gross, U., Kirkpatrick, C., Schubert, H., and Brochhausen, C., "Going beyond histology. Synchrotron micro-computed tomography as a methodology for biological tissue characterization: From tissue morphology to individual cells," *J. R. Soc. Interface* **7**(42), 49–59 (2010).

[23] Huang, S., Kou, B., Chi, Y., Xi, Y., Cao, Y., Cui, W., Hu, X., Shao, Z., Guo, H., Fu, Y., Xiao, T., Sun, J., Zhao, J., Wang, Y., and Wu, J., "In-line phase-contrast and grating-based phase-contrast synchrotron imaging study of brain micrometastasis of breast cancer," *Sci. Rep.* **5**, 9418 (2015).

[24] Zehbe, R., Schmitt, V. H., Kirkpatrick, C. J., and Brochhausen, C., "High resolution X-ray tomography - Three-dimensional characterisation of cell-scaffold constructs for cartilage tissue engineering," *Mater. Sci. Tech. (UK)* **31**(2), 167–173 (2015).

[25] Langer, M., Pacureanu, A., Suhonen, H., Grimal, Q., Cloetens, P., and Peyrin, F., "X-Ray phase nanotomography resolves the 3D human bone ultrastructure," *PLoS ONE* **7**, 8 (2012).

[26] Khimchenko, A., Deyhle, H., Schulz, G., Schweighauser, G., Hench, J., Chicherova, N., Bikis, C., Hieber, S., and Müller, B., "Extending two-dimensional histology into the third dimension through conventional micro computed tomography," *NeuroImage* **139**, 26–36 (2016).

[27] Götz, C., "Comparing absorption and phase contrast modes in micro computed tomography measurements of osteochondral specimens of the human knee," *Masters thesis in Sport Sciences, University of Basel* (2015).

[28] General Electric, Measurement and Control, "Phoenix nanotom m 180 kV / 20 W X-ray nanoCT system for high-resolution analysis and 3D metrology, https://www.gemeasurement.com/inspection-ndt/radiography-and-computed-tomography/phoenix-nanotom-m," (26.09.2016).

[29] Egbert, A. and Brunke, O., "High-resolution X-ray computed tomography for materials research," *Adv. Mat. Res.* **222**, 48–51 (2011).

[30] Khimchenko, A., Schulz, G., Deyhle, H., Hieber, S., Hasan, S., Bikis, C., Schulz, J., Costeur, L., and Müller, B., "Non-destructive phase contrast hard X-ray imaging to reveal the three-dimensional microstructure of soft and hard tissues," *Proc. SPIE* **9797**, 97970B (2016).

[31] Weitkamp, T., Diaz, A., David, C., Pfeiffer, F., Stampanoni, M., Cloetens, P., and Ziegler, E., "X-ray phase imaging with a grating interferometer," *Opt. Express* **13**(16), 6296–6304 (2005).

[32] Rau, C., Wagner, U., Pešić, Z., and De Fanis, A., "Coherent imaging at the Diamond beamline I13," *Phys. Stat. Sol.* **208**(11), 2522–2525 (2011).

[33] Haas, W., Bech, M., Bartl, P., Bayer, F., Ritter, A., Weber, T., Pelzer, G., Willner, M., Achterhold, K., Durst, J., Michel, T., Prümmer, M., Pfeiffer, F., Anton, G., and Hornegger, J., "Phase-unwrapping of differential phase-contrast data using attenuation information," *Proc. SPIE* **7962**, 79624R (2011).

[34] Weitkamp, T., Haas, D., Wegrzynek, D., and Rack, A., "ANKAphase: Software for single-distance phase retrieval from inline X-ray phase-contrast radiographs," *J. Synchrotron Rad.* **18**(4), 617–629 (2011).

[35] Andronache, A., von Siebenthal, M., Székely, G., and Cattin, P., "Non-rigid registration of multi-modal images using both mutual information and cross-correlation," *Med. Image Anal.* **12**(1), 3–15 (2008).

[36] Zanette, I., Lang, S., Rack, A., Dominietto, M., Langer, M., Pfeiffer, F., Weitkamp, T., and Müller, B., "Holotomography versus x-ray grating interferometry: A comparative study," *Applied Physics Letters* **103**(24), 244105 (2013).

[37] Pfeiffer, F., Bech, M., Bunk, O., Kraft, P., Eikenberry, E., Brönnimann, C., Grünzweig, C., and David, C., "Hard X-ray dark-field imaging using a grating interferometer," *Nat. Mater.* **7**(2), 134–137 (2008).

[38] Miller, L. and Dumas, P., "From structure to cellular mechanism with infrared microspectroscopy," *Curr. Opin. Struct. Biol.* **20**(5), 649–656 (2010).

[39] Walton, L., Bradley, R., Withers, P., Newton, V., Watson, R., Austin, C., and Sherratt, M., "Morphological characterisation of unstained and intact tissue micro-architecture by X-ray computed micro- and nano-tomography," *Sci. Rep.* **5**, 10074 (2015).

[40] Wenz, J., Schleede, S., Khrennikov, K., Bech, M., Thibault, P., Heigoldt, M., Pfeiffer, F., and Karsch, S., "Quantitative X-ray phase-contrast microtomography from a compact laser-driven betatron source," *Nat. Commun.* **6**, 7568 (2015).